Fermi National Accelerator Laboratory

Fermilab

FERMILAB-FN-1063-DI

FINAL REPORT: CONCEPTUAL DESIGN OF A 10-MEGAWATT ELECTRON BEAM IRRADIATION FACILITY FOR BIO-SOLID WASTE TREATMENT

Fermi National Accelerator Laboratory
Kirk and Pine Street / P.O. Box 500 / Batavia, IL 60510

Managed by Fermi Research Alliance, LLC for the U.S. Department of Energy Office of Science

DOE / Office of Science Program Office: High Energy Physics

December 12, 2018
Fermi National Accelerator Laboratory
Metropolitan Water Reclamation District of Chicago
FERMILAB-FN-1063-DI

This manuscript has been authored by Fermi Research Alliance, LLC under Contract No. DE-AC02-07CH11359 with the U.S. Department of Energy, Office of Science, Office of High Energy Physics.

Table of Contents

CONCEPTUAL DESIGN OF A 10-MEGAWATT ELECTRON BEAM IRRADIATION FACILITY FOR BIO-SOLID WASTE TREATMENT

J. C. T. Thangaraj, A. Saini, V. Yakovlev, I. Gonin, N. Solyak, R. Dhuley, T. Kroc,

M. Geelhoed, I. Tropin, N. Mokhov, T. Khabiboullline

Fermi National Accelerator Laboratory

Introduction

In this report, a conceptual design is proposed for a 10 mega-watt (MW) electron beam accelerator for wastewater treatment. This is done by applying the latest accelerator technologies developed at Fermilab and within the Department of Energy (DOE) Office of Science laboratory complex. This report expands on previous work on the 1 MW accelerator, which was developed with requirements from Metropolitan Water Reclamation District (MWRD) in Chicago. The full report of the previous effort is available from the Office of High Energy Physics Accelerator Stewardship Program [1].

The explosion in urban population around the world presents enormous challenges for providing and protecting the quality of municipal water supplies. One of the best identified ways to effectively treat municipal water is to use electron beam (EB) irradiation [2-5]. However, despite the technical success of several experimental and pilot programs over the last few decades, EB irradiation is still not in commercial use anywhere in the world. This is primarily due to the lack of high power (typically mega-watt) accelerators to handle large volumes in a practical water treatment plant.

EB TREATMENT REQUIREMENTS

The conclusion of the previous report identified the key features of an optimized and cost effective EB treatment system must include: 1) ability to create the large required EB power; 2) high overall wall plug power efficiency; 3) affordable capital cost for the entire system including the cost of shielded enclosures and beam delivery systems; 4) high reliability and/or redundancy to achieve 24/7 availability; 5) a turn-key industrial solution that does not require expert operators; 6) an optimized process that minimizes the required EB dose (due to the large volumes of materials to be processed); 7) a process that meets all regulatory standards.

BACKGROUND

Initial considerations such as overall EB power requirements, accelerator physical size, cost of shielded enclosures, required wall plug power efficiency, and capital expense (CAPEX) cost/watt, have already determined that normal conducting accelerators are not well suited for wastewater and biosolid applications. As an example, the estimated required electron beam power for treating dewatered biosolid sludge or the pre-anaerobic digester thickened Waste Activated Sludge (WAS) stream in the MWRD Stickney Plant at 2 Million Gallons per Day (MGD) was manageable at 1 MW.

Therefore, MWRD and Fermilab collaborated to complete an OHEP Stewardship funded effort to create a conceptual design for a 1 MW SRF-based electron accelerator (Type 3). The effort included a complete beam physics simulation for the 250 kW accelerator modules that provide 1 MW of combined beam power. An electron gun/cavity configuration that produced simulated

losses of zero was arrived at such that, when statistical errors are included, the loss level is < 10^{-6} of the beam [1].

NEED AND APPROACH

While the 1 MW beam power is sufficient for bio-solid treatment at 1 MGD, an important area of interest for MWRD is improving the ability to remove water from WAS before thickening where the flow rate is higher. In this case, the flows are larger at 8-13 Million Gallons per Day (MGD). Therefore, if a 10 kGy dose is required to improve dewatering, this leads to an EB power requirement for MWRD to be 4-6 MW assuming all the beam is effectively utilized. This means treatment of this waste stream is only addressable with a 10 MW scale accelerator. Motivated by encouraging simulation results for a 250 kW SRF module, the conceptual design of a 10 MW combined beam power system based on 1 MW modules was developed.

The increase in beam power in each module was accomplished by increasing the average beam current in each accelerator module by a factor of four from our previous concept. Although much of the previous work was applicable, such high gun currents and electron beam powers needed additional simulation effort that employed higher statistics to understand loss distributions at the level of 10^{-6} or lower. In these studies, the limits of achievable beam power for such SRF accelerator modules was explored. Other challenges at these high beam powers were RF couplers, RF power sources, beam delivery, and shielding. Of particular note are the challenges associated with windows that separate the clean vacuum of the cavity from the harsh environment of the industrial waste streams at issue. As in previous work, the accelerator design will focus on the concept and feasibility of a very high power industrial Superconducting Radio-Frequency (SRF) electron beam accelerator that leverages recent transformational SRF technology improvements to achieve both reliability and cost targets via a modular approach and an innovative low-cost Radio-Frequency (RF) power source.

Conceptual design for the 10 MW compact SRF accelerator

The conceptual design for a 10 MW electron beam irradiation facility is based on ten identical units of 1 MW linac modules. Each module is designed to deliver a 100mA, 10 MeV CW electron beam based on SRF technology, which is the most cost-effective way to build and operate MW beam facilities. SRF technology enables high accelerating fields with minimum power dissipation and high-duty factor beam operation.

However, achieving superconducting temperatures requires a significant investment in a cryogenic system, which is a cumbersome and large system. This is where Fermilab's novel conduction cooling technique allows one to reach superconducting temperatures without using complex cryogenic systems [6]. This is done with a combination of advanced SRF coatings and compact, industrially available cryo-coolers to maintain the cryogenic temperature for reliable operation of the SRF cavity. This patented technology was recently demonstrated at the IARC facility. Conduction cooling technology achieves superconducting temperatures without requiring a cryogenic system which is cumbersome and complex.

For the objective of this report, the limited cryogenic capacity of cryo-coolers (2 W) places stringent tolerances on power dissipation in the SRF cavity. Consequently, it puts a strict limitation on the beam loss in SRF section. Therefore, the goal is to develop a baseline configuration with a minimal

uncontrolled beam loss in the linac optics design. Because of the identical nature of each module, only the 1 MW machine will be discussed in most parts of the report.

To be specific, the conceptual design of a 1 MW beam power module that has a 4 ½ cell, 650-MHz, elliptical Nb cavity, coated inside with Nb_3Sn, and powered by an RF source with ~80% efficiency and a target cost of $4/W is to be focused on. Elliptical SRF cavities at 650 MHz are a natural choice for this application since this is a frequency already chosen for Office of Science applications that represents a good balance between physical size; cavity cost; large apertures leading to low beam losses; and low expected cryogenic load during CW operation. Each independent module will deliver ~10 MeV electrons in Continuous Wave (CW) operation. This report addresses key design aspects of the basic module to validate or improve the initial vision and determine the performance requirements of emerging technology.

The team began by modifying the physics calculations and simulations to understand how higher current beam (100 mA average, > 1 A peak) can be generated at the cathode, accelerated away from the space-charge regime and transported through the linac to 10 MeV with a total power of 1 MW all the while maintaining the beam losses at or below 10^{-6}. This does not include particle losses that happen outside the SRF cryomodule that does not contribute to the heat budget such as scrapers. As mentioned above, IARC's previous work indicated that a 650 MHz cavity coated with Nb_3Sn cavities operating at 4 K CW, with ~10 MeV/m gradient can accelerate 25 mA electron beams corresponding to 250 kW output power per module with insignificant loss. Finally, a preliminary estimate for the Type 4 target capital and operating costs for the first article and in production will be discussed.

IARC focused on design solutions for high current cathodes, very high-power couplers, low cost RF, and careful beam transport with an overarching goal to minimize beam loss – a stringent requirement in an SRF accelerator for MW power levels. An acceptable target is a loss of $< 2 \times 10^{-6}$ of the beam on cold cavity surfaces corresponding to 2.0 W at 4 K. The team estimated that an optimized, magnetically shielded 650 MHz Nb3Sn coated 4 ½ cell cavity can achieve dynamic RF losses ~ 2.5 W at 4 K based on measurements of similar 1.3 GHz cavities [6]. The goal is a 1MW module cooled by several high capacity, high reliability commercial cryocoolers without the use of Liquid Helium. The MTF for current cryocoolers is between 40000-70000 hours making them ideal for industrial use. This approach permits use of a simple cryostat and a completely sealed helium system—both are key items for simple turn-key industrial operation.

In summary, IARC envisioned a novel SRF-based, 10-MeV, 10-MW, industrial electron accelerator that consists of ten modules each containing a 4 ½ cell, 650-MHz, elliptical Nb cavity, coated inside with Nb3Sn, and powered by an RF source with 80% efficiency. Each independent module will deliver 1 MW of 10 MeV electrons in Continuous Wave (CW) operation. This modular approach is attractive to MWRD because it can provide a straight-forward path to scaling to higher powers and can provide operational reliability via redundant modules.

THE 1 MW CRYOMODULE DESIGN FOR A 10 MW ACCELERATOR

Figure 1 is a schematic of the baseline 1 MW linac module. It is composed of three main sections which are modularly connected:

- Injector
- Main Accelerating Section
- Beam Delivery System

Each of these sections is treated with inputs from the previous section and iteratively designed. As an example, the optics design of the main accelerating section was made using an input beam distribution generated from the RF gun while the RF gun design was made to deliver a high-quality beam with an optimal energy that ensured a maximum capture through the accelerating section. The final design of the linac is the result of several iterations accounting for different aspects of the design considerations. A detailed description of each section layout follows.

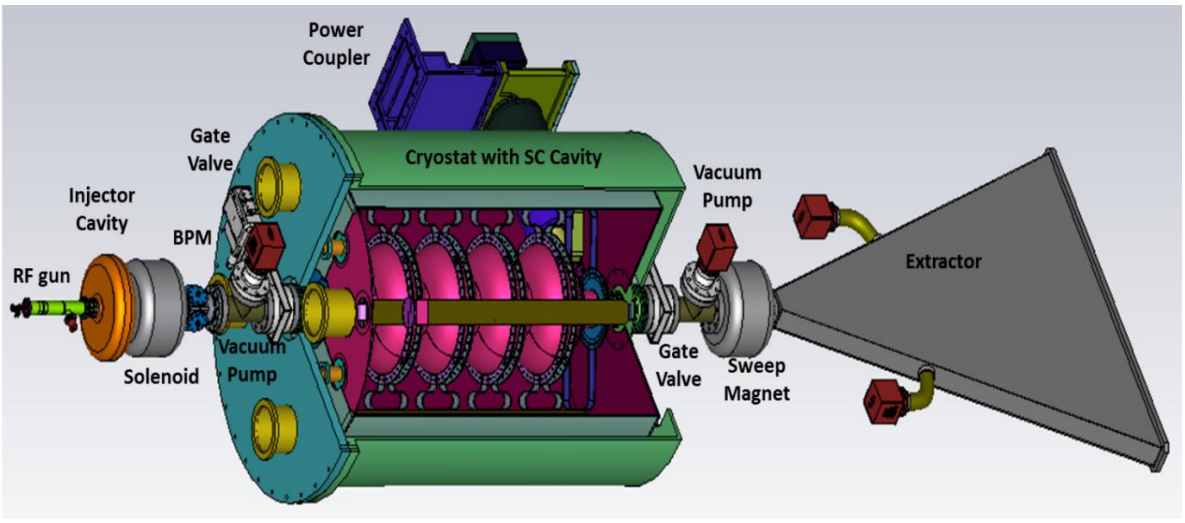

Figure 1 Schematic layout of a 1 MW linac module for the MWRD facility. Ten identical modules will be used to deliver 10 MW beam.

INJECTOR

In recent years, SRF injection schemes [9] have been widely used in new proposals and ongoing projects throughout the world. An SRF injector typically includes a photocathode placed inside an SRF accelerating cavity. Because particles are emitted inside the accelerating cavity, they are quickly captured and accelerated; therefore, a high-quality beam is delivered at the output.

However, this scheme also poses severe technical challenges; for example, particles that are not captured contribute to additional power dissipation in the cavity. In addition, as the cathode operates in the normal conducting state, it acts as a heat source while the SRF cavity serves as a sink. Thus, black body radiation coming from the cathode is deposited on the cavity. The heat load of the cavity is limited due to the cooling efficiency of the cryo-coolers. Therefore, an external beam injection scheme was selected for the following reasons:

- High current emission from the cathode increases the possibility of evaporation of the cathode material. In the case of internal injection, this material may deposit to the cavity surface and degrade its quality-factor. External injection reduces the likelihood of material deposition on the surface of the cavity.
- A large cathode could be built for an external injection scheme that reduces the surface

current density. A lower surface current density not only improves the longevity of a cathode but also reduces material evaporation from the surface of the cathode.

- Only a small fraction of lateral heat radiation from the cathode reaches the SRF cavity in the external injection scheme.
- The fraction of the beam not captured gets lost in the normal conducting section. This reduces the thermal load on the superconducting section.
- An external injection usually requires only a modest vacuum.

The proposed external injection scheme for the MWRD facility includes a thermionic cathode-based RF gun and an injector cavity that provides a pre-acceleration to the beam before it enters the superconducting section. Figure 2 is a schematic of the injector layout. The RF gun resonator is installed at base of the cathode-grid assembly. A grid is used to gate the electron emission. A single cell injector cavity is placed just downstream of the gun-grid assembly. The injector section must deliver a high-quality beam to the SRF section. Thus, the gun design facilitates operation not only at the fundamental frequency of 650 MHz but at the second harmonic if needed to obtain a short bunch length.

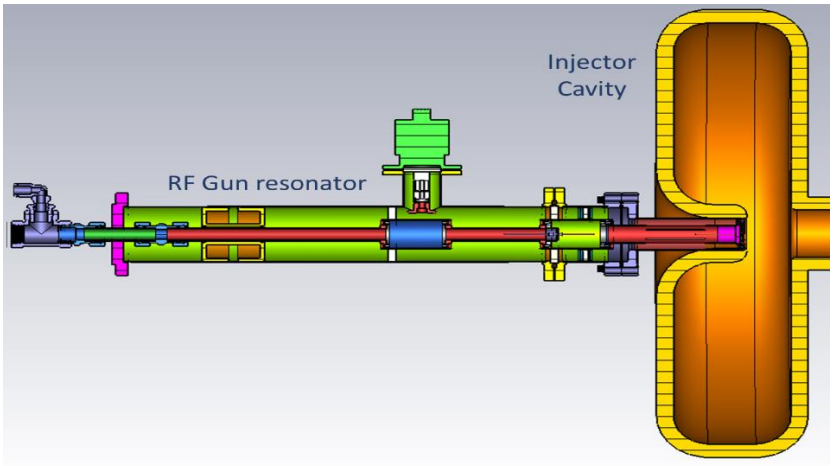

Figure 2 Schematic of the injection scheme that includes a RF gun and an injector cavity.

To match the injection energy at the entrance of the main accelerating section, special design considerations of the RF gun and injection cavity were considered to accelerate non-relativistic low energy electrons. In addition, operating parameters such as DC voltage, RF voltage, phase interval of gun were also optimized to deliver a well-focused beam. A detailed discussion of the RF gun and injection cavity designs are presented in following sections.

RF GUN

Operational experience gained through several ongoing projects [7-10] showed that RF guns based on thermionic cathodes, are cost effective, simple and reliable. They can be operated in various regimes with minimal backward bombardment of the electrons and can deliver a high-quality beam with low energy and phase spread among particles. In addition, they are ideal for applications that require high average beam current and long lifetime. These features make the thermionic-cathode RF gun a preferred choice for the project. Figure 3 shows the proposed layout of the RF gun for the

MWRD linac.

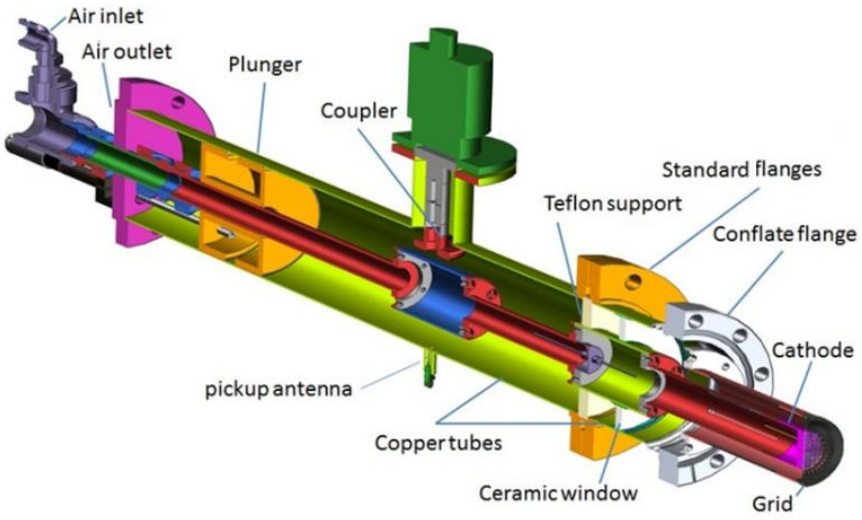

Figure 3 Layout of proposed RF gun.

The design has three independent parts: the RF resonator with power coupler, the thermionic cathode, and the grid assembly. As shown in figure 4, the cathode unit is mounted to the RF gun resonator by a flanged connection and can be separated from the gun during maintenance. The proposed design concept facilitates easy maintenance and assembly. In addition, this facilitates rapid repair or replacement of a part during operation and, therefore, improves beam availability during operational hours. Beam availability and reliability are vital features of a successful accelerator facility.

The standard series barium tungsten dispenser cathode with diameter of 0.5 inch at operation temperature 950-1200 ^{0}C is proposed to be used. This kind of cathode is commercially available [11]. The distance between the cathode surface and the grid surface is 0.6 mm. A bellows is to be used as part of the outer conductor of the RF gun for mechanical adjustment of the cathode-grid distance. As shown in figure 4, the tungsten grid assembly is mounted to the flange, which is welded to the Injector cavity.

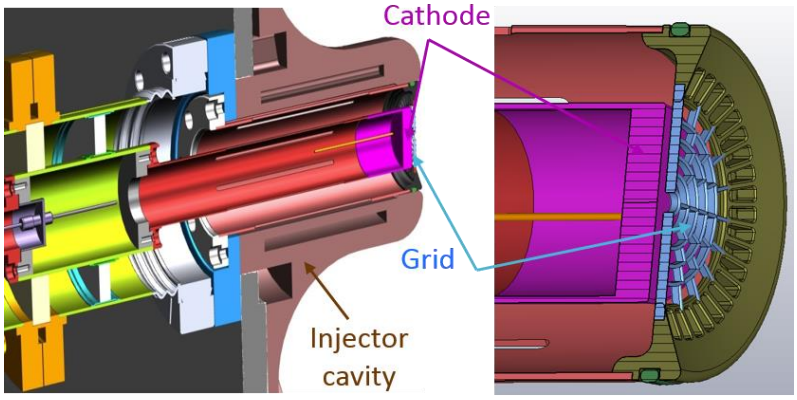

Figure 4 Cathode-grid assembly

ELECTROMAGNETIC DESIGN OF GUN RESONATOR

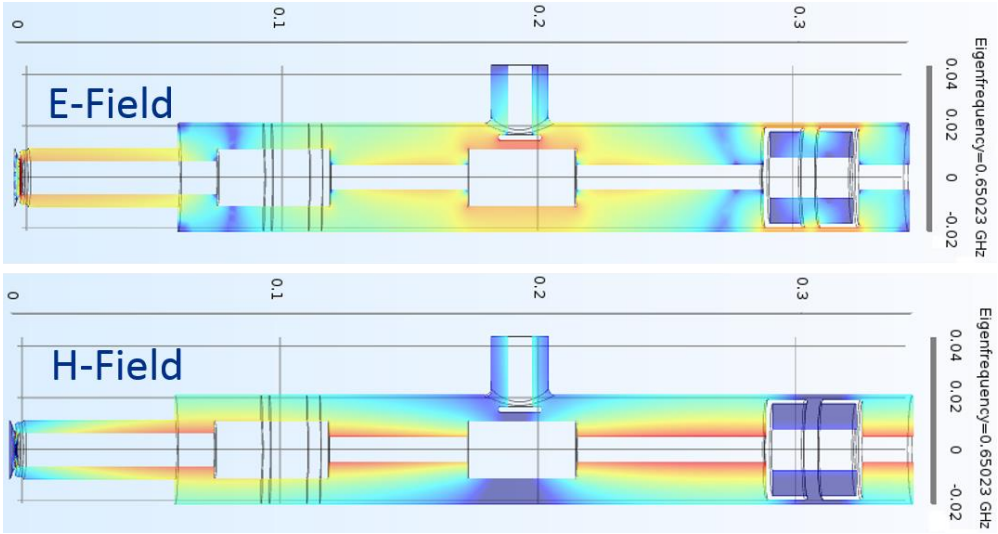

Figure 5 Electric (top) and magnetic (bottom) field masp in the RF Gun resonator. The red color in the map corresponds to the maximum field strength while blue color indicates a lower strength of the field.

RF design of the gun resonator was performed using COMSOL [12]. It operates at a frequency of 650 MHz and at a nominal voltage of 2.85 kV. Figure 5 shows the electromagnetic field map in an optimized geometry for nominal RF parameters. The magnetic field is mainly concentrated in the inner-conductor while the peak electric field was obtained in proximity to the power coupler tip. The plunger position in the gun cavity is adjustable and can be used for fine tuning of the cavity resonance frequency.

One of the major concerns associated with a normal conducting RF gun is power dissipation. For the proposed design, the estimated total power dissipation in the gun resonator for a nominal operating RF voltage of 2.85 kV is about 130 W, while it is 2 W in the tungsten grid. Most of the loss happens in the inner-conductor, which can water-cooled [13].

INJECTOR CAVITY

As stated earlier, an injector cavity is deployed to provide pre-acceleration to the beam. This must have a sufficient beam velocity at the entrance of a β~1 SRF cavity to maximize the beam capture through it. Thus, the primary objective of the optimization is to obtain a maximal accelerating gradient with manageable power loss. Furthermore, the design considered feed-back from the beam dynamic simulation to determine an optimal accelerating gradient needed from the injection cavity.

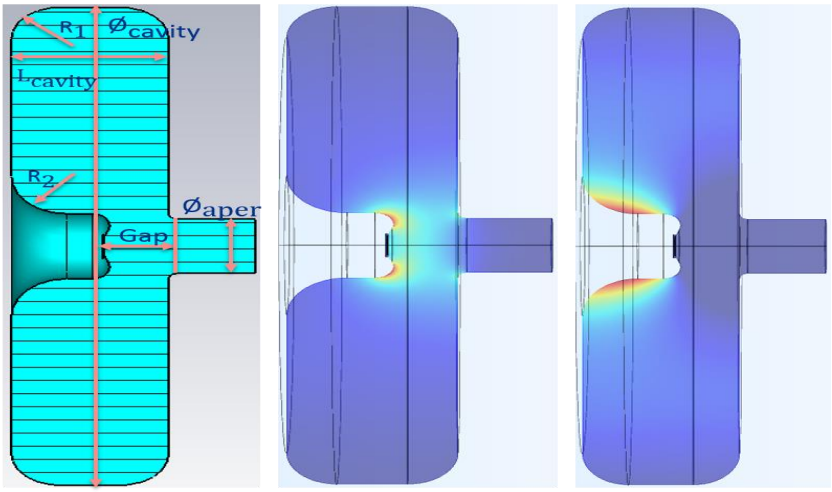

Figure 6 Geometry (left) and electric (middle) and magnetic field (right) distribution in the injector cavity for nominal parameters.

Parameter	Value, mm
$Ø_{cavity}$	308
$Ø_{aperture}$	35
R_1	20
R_2	24
Gap	29.6
L_{cavity}	68.2

Figure 7 Geometrical parameters of injector cavity

The injector cavity design was optimized using COMSOL. Geometrical parameters that were varied to obtain the design gradient were longitudinal length *"L"* and accelerating gap length *"Gap"*. In addition, the cavity radius *"$Φ_{cavity}$"* was used to tune the operating frequency to *650 MHz*. Figure 6 depicts critical geometrical parameters and field distributions in the cavity. Geometrical and RF parameters of the injector cavity are summarized in Figures 7 and 8, respectively.

Parameter	Unit	Value
Frequency	MHz	650
Voltage (amplitude)	kV	300
R/Q	Ω	178
Q	Ω	19000
R_{sh}	MΩ	3.4
Losses in cavity	kW	17
E_s, max	MV/m	18.9

Figure 8 RF parameters of the injector cavity

BEAM DYNAMICS STUDY IN RF GUN

A beam dynamics study of the injector section was performed using SMASON [14]. Modeling was performed by simulating the cathode, grid, and injector cavity altogether. An RF voltage with an operating frequency of 650 MHz and a DC voltage were applied to the cathode to generate a designed beam current of 100 mA. Thus, voltage at the cathode U at a time t is expressed as:

$$U(t) = U_d + U_a \cos(\omega t + \varphi) \qquad (1)$$

where U_d is the constant DC voltage, U_a is the amplitude of the RF voltage, ω is the angular operating frequency, and φ is the phase shift between the bias RF voltage and RF fields in the injection cavity. RF voltage (U_{RF}) in the injector cavity was modelled in SMASON using the following expression:

$$U_{RF}(t) = U_0 \cos(\omega t) \qquad (2)$$

where U_0 is the static field. This field approximation performs well in regimes where the cathode size is much smaller than the operating wavelength of the cavity.

To achieve the design objectives of 100 mA beam current, minimization of energy and phase spread among particles, and higher output beam energy downstream of the injection section, U_a, U_d, φ, U_0 and the geometry of cathode-grid assembly were optimized. Figure 9 shows a simplified 2D model of the cathode-grid assembly that was used in SMASON. Space charge effects were also accounted for in the simulation.

The optimization process includes adjustment in geometry and RF and DC voltages at the cathodes to obtain an average beam current of 100 mA. Then, for a given set of voltages, phase φ and U_0 were optimized to achieve optimal parameters at the end of the injector section. Final parameters after the optimization are summarized in Figure 10.

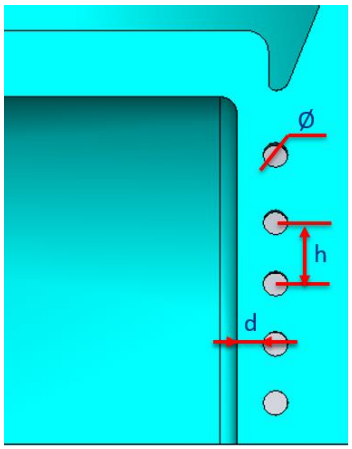

Figure 92D SMASON model for the cathode-grid assembly. Parameters involved in geometry optimization were also highlighted.

Grid optimization:

- number of wires
- cathode-grid distance *(d)*
- diameter of grid rings *Ø*
- distance between wires *(h)*

To provide:

- emission uniformity
- grid transparency
- minimal losses on the grid

Parameter	Unit	Value
Input to simulation		
Frequency	MHz	650
Cathode diameter	inch	0.5
Beam current	mA	100
Current density	A/cm^2	2.35
Output from simulation		
DC voltage (U_d)	kV	2.6
RF gun voltage (U_a)	kV	2.85
RF voltage in Injector Cavity (U_0)	kV	300
Output Energy	keV	275
Energy rms size	%	3.8

Figure 10 Final parameters obtained from SMASON after beam dynamics optimization.

The optimal RF phase interval between the fields in the Gun resonator and the injector cavity was found to be 85^0. It provides an RMS energy spread of 10 keV and an RMS phase spread of 78 ps in a 100-mA bunch. Figure 11 shows beam parameters at the end of injection section. A 3D simulation code, MICHELLE, will be used to finalize the design of the injection section. However, a previous study (as shown in appendix-I,) suggested good agreement between MICHELLE and SMASON [14].

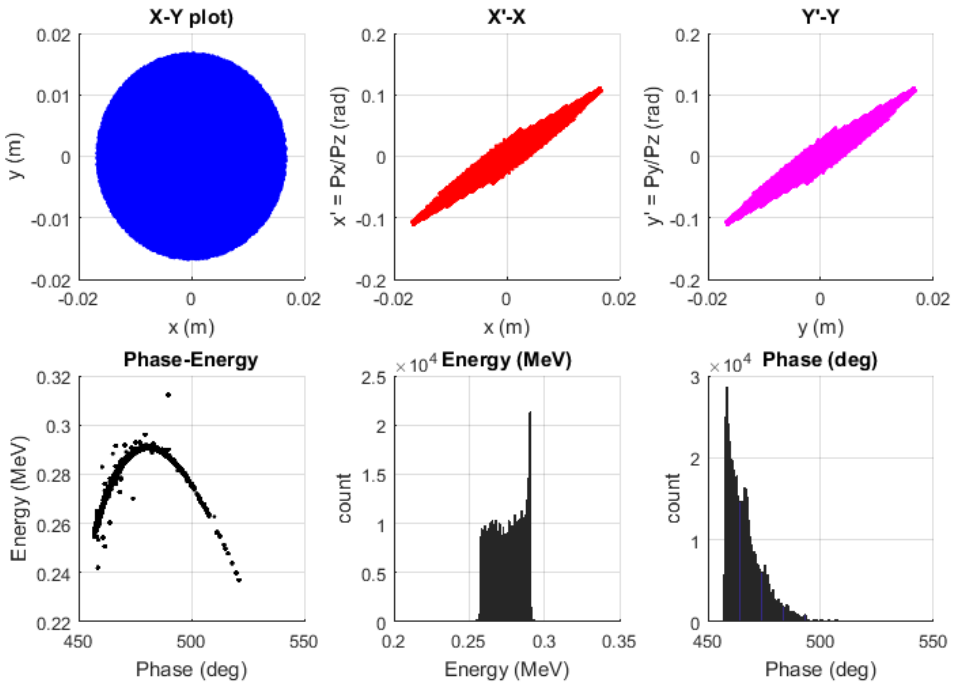

Figure 11 Beam parameters at the end of injection section.

MAIN ACCELERATING SECTION

This section reports simulation results of the main accelerating section using the beam dynamics code TRACEWIN [15]. TRACEWIN is a multi-particle tracking code that can compute both 2D and 3D space charge effects. This allows the construction of beamline elements using an existing library as well as implementation of 3-D fields from an external field map obtained from electromagnetic simulation of elements. TRACEWIN can generate a Gaussian beam distribution in 6-D phase space from user-defined Twiss parameters and beam emittance. Furthermore, it can read a real distribution from an external file.

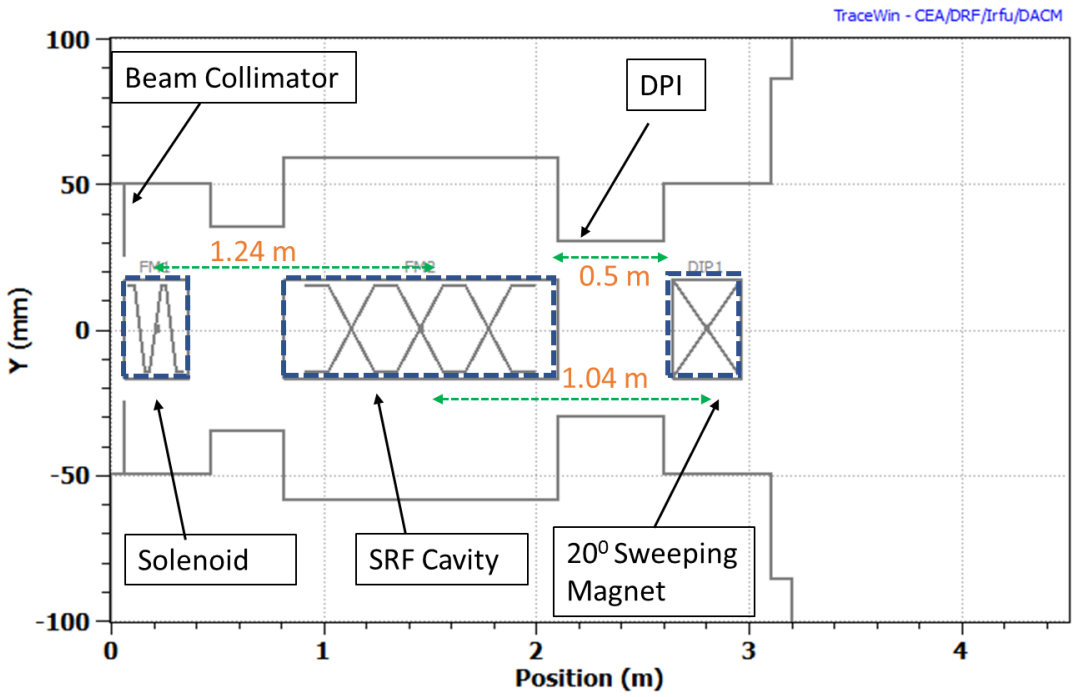

Figure 12 A schematic of the beamline highlighting critical elements and their center to center separation. DPI stands for Differential Pumping Insert. The schematic includes a solenoid, a SRF cavity and a 20⁰ sweeping magnet. The minimum aperture of 60 mm in the line is associated with the differential pumping insert. Design ideas and specifications of the beamline elements are discussed in detail below.

SPECIFICATION OF BEAMLINE ELEMENTS

SOLENOIDAL FOCUSING MAGNET

The beam particles emitted by the gun have large diverging angles. Consequently, the transverse size starts to grow very rapidly along the beamline. Thus, a solenoidal focusing system was used to constrain the beam sizes in horizontal and vertical planes. Physical length and aperture of the solenoid are 120 mm and 90 mm respectively. A large aperture ensures no beam interception in this region. However, a large aperture results in long axial fringe fields. These fields can disrupt not only beam dynamics but also the effective operation of the SRF cavity located in proximity to the solenoid. Thus, to minimize fringe fields, the solenoid might include two bucking coils in addition to the main coil. The bucking coils will produce magnetic fields in the opposite direction to the main coil, thereby limiting the fringe fields. This approach is widely used for superconducting solenoids [16,17] where the focusing period is relatively short and SRF resonators are placed in proximity to the solenoids. Another option is to encircle the solenoid with an iron yoke, thus shielding its fringe field. To save space, a beam position monitor (BPM) and steering correctors are proposed to be installed at the center of the solenoids. Steering correctors serve to correct the beam trajectories in the horizontal and vertical planes while compensating for uncertainties in the solenoid magnetic axis positioning.

Steering correctors were designed to deliver a maximum kick *(θ)* of *10* mrad. This kick is sufficient to shift the beam by 10 mm from the axis of the cavity. Thus, the design specification for the maximum integral field (BL) in the corrector (using equation 3 where $B\rho$ is beam rigidity) is: 0.2 mT-m.

$$\theta = \frac{BL}{B\rho} \quad (3)$$

ACCELERATING SUPERCONDUCTING RADIO FREQUENCY CAVITY:

A 650, MHz, β_g =1, elliptical shaped SRF cavity was designed to accelerate the beam from an initial beam energy of 275 keV to 10 MeV. The choice of an operating frequency of the cavity is made with considerations of both practical and fundamental aspects which are summarized below:

Maximization of Accelerating field: To develop a compact and cost-effective accelerator, an unprecedented "conduction cooling" technique will be used to cool down the cavity to the operating temperature of 4K. The availability of the refrigeration puts a stringent limit on the surface power dissipation (P_D) in the cavity which is estimated using following expression:

$$P_D = \frac{1}{2} R_s \int_s H^2(s) ds \; ; (4)$$

where R_s is the surface resistance, *S* is the surface area of the cavity and *H* is the magnetic field amplitude. The BCS surface resistance is proportional to the square of the frequency while the surface area of the cavity is inversely proportional to the square of the frequency. In this regime, two cavities operating at different frequencies but at same field amplitude will have same power dissipation. However, energy gain in a cavity is

$$E_{gain} = q \int_0^L E_z(z) e^{i(\omega t - kz)} dz \; ; (5)$$

where E_z is the longitudinal electric field along the cavity and *L* is the length of the cavity and given as

$$L = \frac{1}{2} N_{cell} \beta_g \lambda ; (6)$$

where β_g is the relative particle velocity, λ is the operating RF wavelength in free space and N_{cell} is the number of cells in a cavity. Equations (5) and (6) show that lowering the operating frequency results in a longer cavity and therefore higher energy gain. To achieve the same energy gain in a shorter (higher operating frequency) cavity, the field amplitude will have to increase. This, in turn, will also increase power dissipation in quadrature. As stated earlier, use of cryo-coolers puts stringent tolerances on the power dissipation. Thus, one prefers 650 MHz frequency to 1.3 GHz.

Large Transverse Acceptance: The transverse dimension of a TM mode operating accelerating cavity is inversely proportional to the operating frequency. A lower frequency results in a large aperture, which reduces the likelihood of the beam loss on the cold surface.

Low Power Dissipation due to Higher Order Modes (HOMs): As stated earlier, a low operating frequency implies a large transverse aperture and, therefore, higher frequency modes easily propagate out of the cavity. This in turn, reduces the possibility of mode trapping and hence minimizes the power dissipation in the cavity. In addition, HOMs were coupled with the power coupler, which further reduces power dissipation at the cold surface. The design exhibits a regular and sparse beam spectrum that further reduces the likelihood of a HOM resonance excitation.

Large longitudinal acceptance: A beam is injected into the accelerating structure with well-defined phase with respect to sinusoidal time varying accelerating field. This phase must be maintained to achieve a continuous acceleration along the cavity. Because the beam is an ensemble of a large number of particles with a finite energy and time spread, particles with large energy and time spread with respect to the reference particle will slip on the field and will ultimately be lost inside the cavity. A lower operating frequency implies a large RF separatrix and ensures maximum capture of particles. A lower operating cavity frequency is preferable for the beam with a longer longitudinal length.

Practical Aspects: A cavity with low operating frequency is large in dimension; therefore, its handling becomes difficult and expensive. Thus, the selection of the operating frequency of the cavity is a compromise between operational requirements and practical factors. For this project, IARC chose 650 MHz frequency, which is a natural choice for this application since it is a frequency already chosen for the Office of Science PIP-II project and extensive development work has already taken place. This, in turn, allows one to leverage the same ancillary components (wherever they apply), such as tuners, RF components etc., reducing R&D cost.

After making the choice of the geometrical beta and the operating frequency, the shape of the cavity was optimized to achieve maximum acceleration and minimum power dissipation. The cavity will operate in pi -mode and is composed of 4.7 cells. Length of the regular cell is calculated using:

$$L = \frac{1}{2}\beta_g \lambda; \quad (7)$$

The particle velocity at the entrance of the cavity is β =0.75 for a cavity designed at β_g=1. This implies that particles take longer to cover the first regular cell and therefore might be out of phase, while decelerated particles, especially at low energy, could get trapped and oscillate back and forth in the cavity until they experience the correct RF phase. In the worst case, this process may lead to a beam loss on the cold surface of the cavity. To fix this problem, the first cell of the cavity is made only 0.7 times the regular cell length. In the first cell, electrons receive sufficient acceleration to become relativistic and therefore no phase slippage occurs in rest of the cavity. This arrangement ensures maximum beam capture and efficient acceleration. The choice of the first cell length was made after several beam-dynamics simulations; it was observed that this length was optimal for this

injection energy. Also, geometrical parameters of the cavity were optimized to minimize field enhancement factors, E_p/E_{acc} and H_p/E_{acc} using COMSOL. Figures 13 and 14 show field distributions in the SRF cavity. Note that fields were normalized to achieve a total of 10 MeV energy through the cavity. RF parameters of the cavity are summarized in Figure 15.

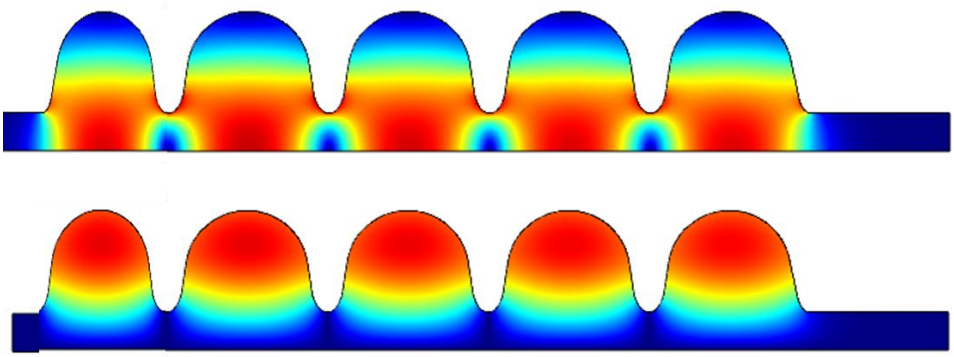

Figure 13 Electric (top) and magnetic field (bottom) distribution along the cavity for nominal accelerating gradient of 10 MV/m. Red color indicates strong field amplitude while blue corresponds to weak field.

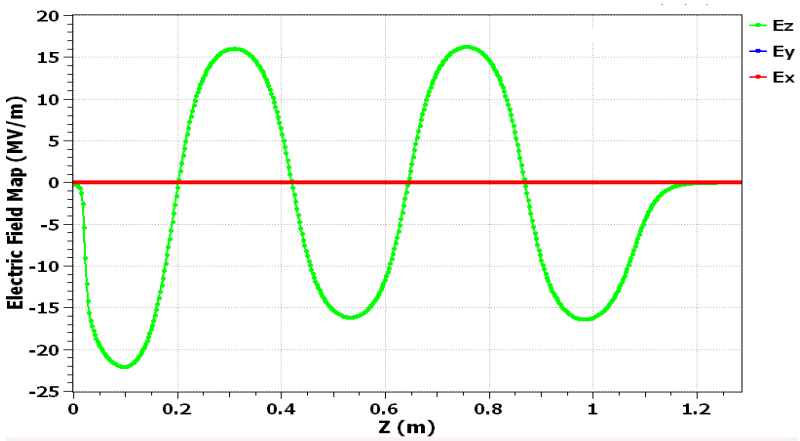

Figure 14 Fields along the axis of cavity. Longitudinal fields are normalized to achieve 10 MeV energy gain in the cavity.

Parameter	Unit	Value
Operating Frequency	MHz	650
R/Q	Ω	528
G	Ω	297
Energy Gain	MeV	10
E_p/E_{acc}	-	2.4
H_p/E_{acc}	mT/(MV/m)	5.5
Active Length	mm	1.0

Figure 15 RF parameters of 4.7 cell elliptical shape 650 MHz SRF cavity

RF POWER SOURCE FOR THE ACCELERATING CAVITY

Since losses in the superconducting acceleration structure are very small, a total of 1 MW of RF input power is required for beam acceleration. A small additional amount (e.g. 10%) of the RF power will be required for control and regulation. A magnetron-based RF source operating in injection-locked mode is envisioned to provide operational power of ~1MW in the CW regime for a 650 MHz superconducting cavity. The phase-locking is done by a reflected wave having an amplitude of 40 % of the incident wave. As discussed elsewhere [18], recent study suggests operating in an injection-locked mode offers a higher efficiency (typically in range of > 80%) compared to klystrons and IOTs, which offer 65% efficiency and solid-state RF sources, which are 50% efficient at 650 MHz. Regarding lifetime, the magnetron lasts between 2000 and 4000 hours while IOTs and klystrons can last up to 50000 hrs [19-21]. However, use of the magnetron simplifies the overall design by avoiding large RF-circulators and thus is simpler to operate.

Note that, $Q_{ext} \sim U/(R/Q * I_{beam})$ for a beam current of 100mA, energy gain of 10 MeV and, R/Q ~500 Ω is about 2×10^5, which results in a bandwidth of the cavity equal to ~3.25 kHz. This implies that the bandwidth of the cavity is much higher than the microphonics that typically lay in range of a few tens of Hertz. The bandwidth of a magnetron is much higher than the cavity bandwidth; this, in turn, eliminates the need for fine tuning the cavity. Furthermore, precise amplitude and phase control of the RF are not mandatory, as there is not a requirement for precise control of the accelerator output energy. It is likely that beam loss control in sweeping magnets may be what sets the overall energy spread requirements. Figure 16 shows a schematic of a conceptual RF transfer line for a 1MW linac module.

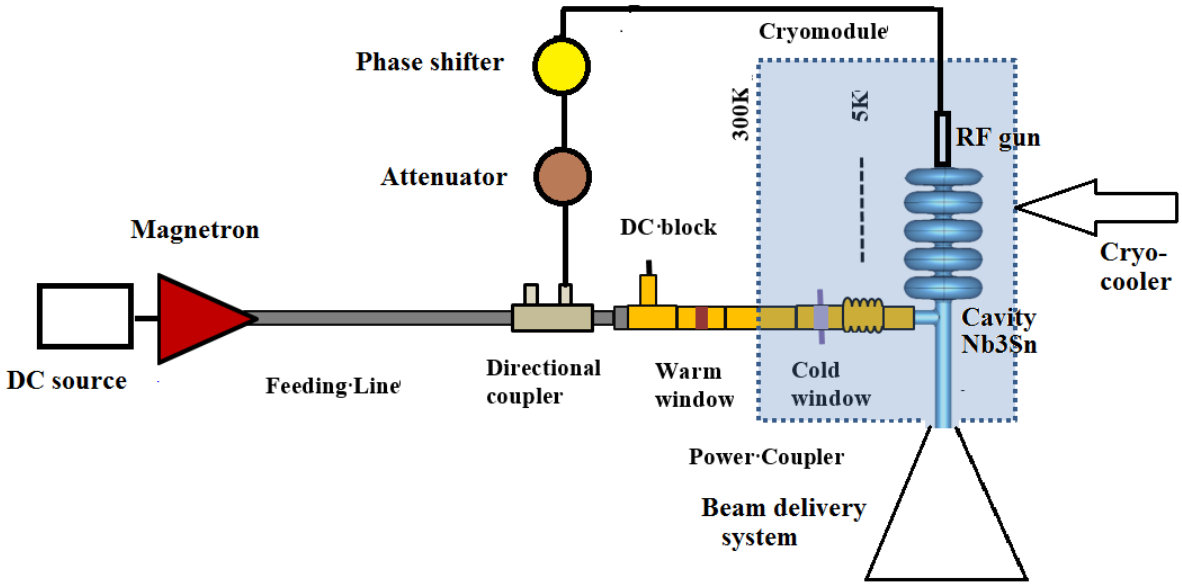

Figure 16 Schematic of conceptual RF transfer line utilizing a magnetron-based RF source. In the above diagram there are three cryocoolers which are not shown for the ease of illustration.

SWEEPING MAGNET DESIGN

A sweeping magnet is placed downstream of the SRF cavity to facilitate the beam scan in the horizontal direction. It is designed to provide a maximum deflection of 20^0 to a 10 MeV electron beam. The magnet length is 325 mm and it provides a maximum integral field of 4.16 mT-m. The aperture of the magnet is 100 mm. The choice of the aperture is made to avoid any potential beam loss across the magnet. The beam width in the vertical direction is sufficiently large and, therefore, beam scanning is not required in this direction.

DIFFERENTIAL PUMPING INSERT (DPI)

The reliable, high performance of the SRF cavity demands a low dust environment to avoid any surface contamination. This, in turn, requires an ultra-high vacuum (UHV) in the SRF section. However, the room temperature section just downstream of the SRF cavity is to be a high vacuum (HV) environment with a characteristic pressure in the ~10^{-8} Torr range. This is driven mainly from a large flux of scattered/reflected particles. To avoid the flux of gas condensing on the cold surface of the SRF cavity, a separation of HV and UHV regions was accomplished in the beamline using the Differential Pumping Insert (DPI) section. This is a low-conductance 0.5m region with an aperture of 60 mm. The volume at the middle of the DPI is pumped by a 100 1/s ion pump. The DPI is electrically isolated such that any beam loss at the aperture restriction may be measured.

Because the SRF cavity operates at 4K, it acts like a sink for the lateral radiations coming from the room temperature sections at both ends of the cavity. Consequently, thermal load of the cryostat is increased. The radiative heat transfer from one surface to another is expressed as the following:

$$Q_{1\to2} = \frac{\sigma(T_1^4 - T_2^4)}{\frac{1}{A_1 F_{1\to2}} + \frac{1-\epsilon_1}{A_1\epsilon_1} + \frac{1-\epsilon_2}{A_2\epsilon_2}}; \quad (5)$$

where $Q_{1\to2}$ is radiative power transfer from surface *1* to surface *2, T*, ε and *A* are temperature, emissivity, and area, respectively. $F_{1\to2}$ is view factor, which determines the fraction of radiation from surface 1 that is reaching to surface 2. Assuming both surfaces are perfect black bodies i.e. $\varepsilon_1 = \varepsilon_2 = 1$, the maximum radiation power deposited (i.e. $F_{1\to2} = 1$) at 4 K from the 50 mm radius beam pipe at 300 K from the surface is *3.6 W*. However, insertion of the DPI results in a lower view factor. Thus. actual power deposited on surface of the cavity is expected to be below 1W. A similar study for a 650 MHz cavity has been presented elsewhere. [22]

BEAMDYNAMICS SIMULATION STUDIES

A preliminary beam optics study was performed to show the feasibility of the concept using the beam distribution received from an SMASON simulation to estimate initial Twiss parameters and beam emittances. Using these parameters, a six-dimensional Gaussian distribution of 10^6 macro-particles was created and tracked through the beamline.

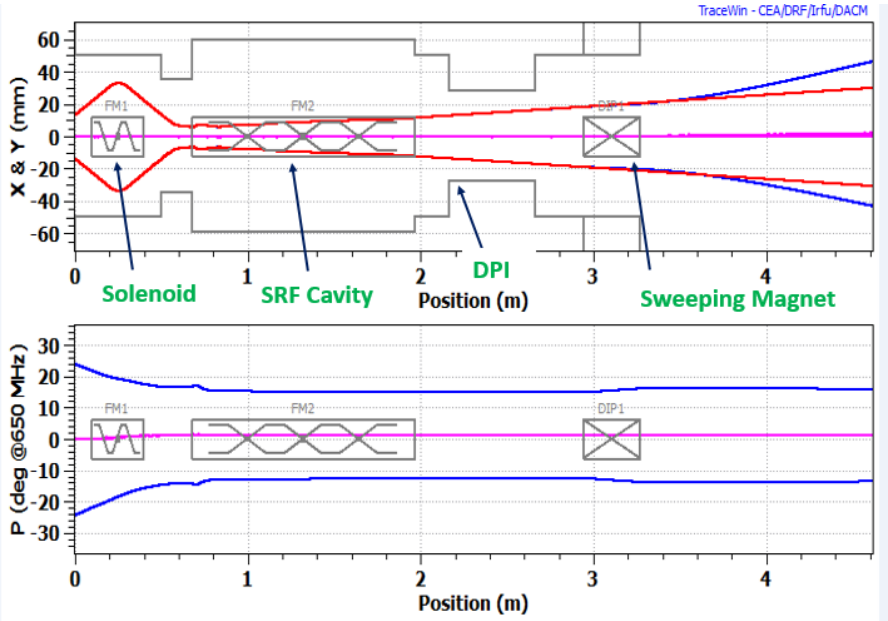

Figure 17 3 sigma beam envelopes in (top) horizontal (blue), vertical (red) and (bottom) longitudinal planes along the beam transport line.

Figure 17 shows 3σ beam envelopes in transverse and longitudinal planes. It can be observed from the figure that the beam emerging from the RF-gun section is diverging very rapidly in the transverse planes. Thus, a solenoid was placed immediately after the injection section. This provided initial transverse focusing to match the beam at the cavity entrance. The cavity was set to negative RF phase relative to crest so that earlier particles experience lower accelerating field than later particles. This leads to a velocity modulation and, therefore, bunching of the beam. The beam became nearly relativistic immediately after the first cell of the cavity. Thus, its longitudinal size remained constant for the rest of the section. Accelerating field in the first cell of the cavity was higher than the rest of the cells. This is done to avoid phase slippage, maximizing beam capture across the cavity. A 20^0 bending magnet was placed near the end to create a raster system that sweeps the beam across the window in the horizontal direction. The final beam energy was 10 MeV. Figure 18 shows the output beam phase space at the end of the beamline. The normalized particle density along the beamline is displayed in Figure 19. Note that there is a possibility of localized beam loss using a beam scraper just downstream of the injector section. This will intercept particles with large transverse position, therefore limiting beam loss in the SRF section. These are localized beam losses at the normal conducting region i.e. outside the SRF section and can therefore be managed by water cooling.

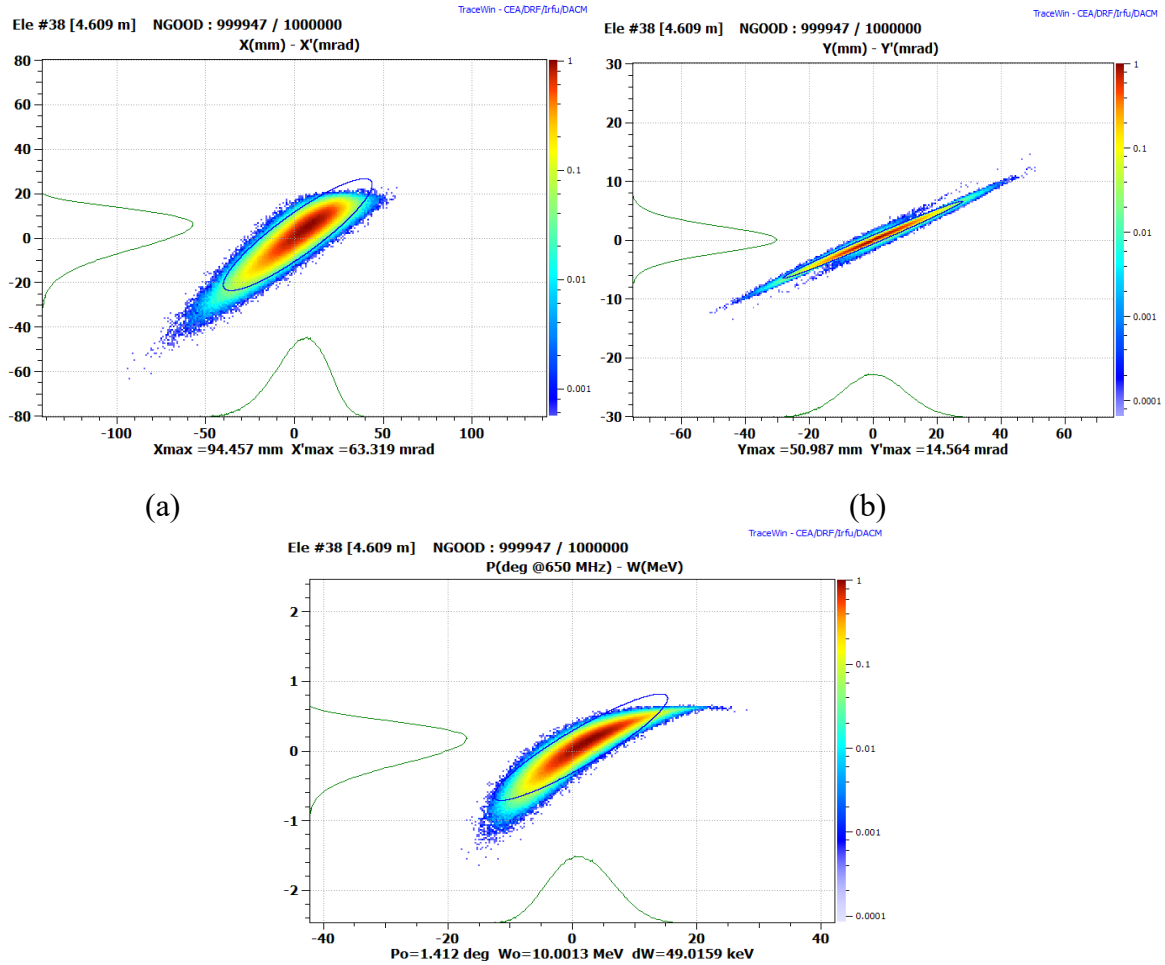

Figure 18 Output beam distribution in (a) horizontal, (b) vertical and (c) longitudinal phase space at the end of the beamline.

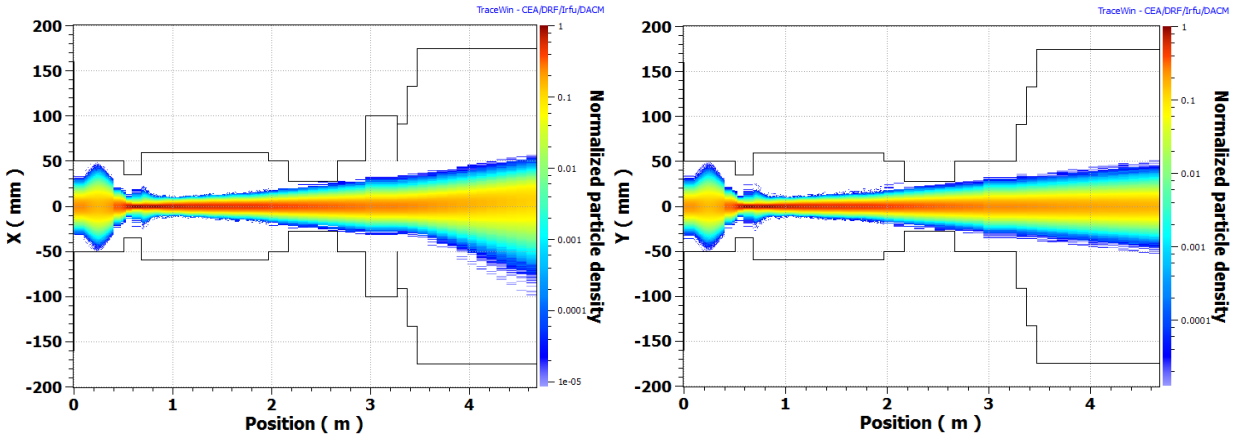

Figure 19 Normalized beam density along the beamline in (a) horizontal and (b) vertical planes.

BEAM DELIVERY SYSTEM

This section reports on the shielding study performed to design an extraction system for a 100 mA, 10 MeV linac. Figure 20 is a layout of the extraction system. The downstream window was optimized to minimize beam induced energy deposition density and back-scattering of particles to the SRF cryomodule. Note that a total heat load contribution from the back-scattered particles should not exceed more than 1 W at 4K and 10 W at 70 K to continue a reliable operation of the linac. Cooling, mechanical, and longevity aspects were accounted for in this optimization.

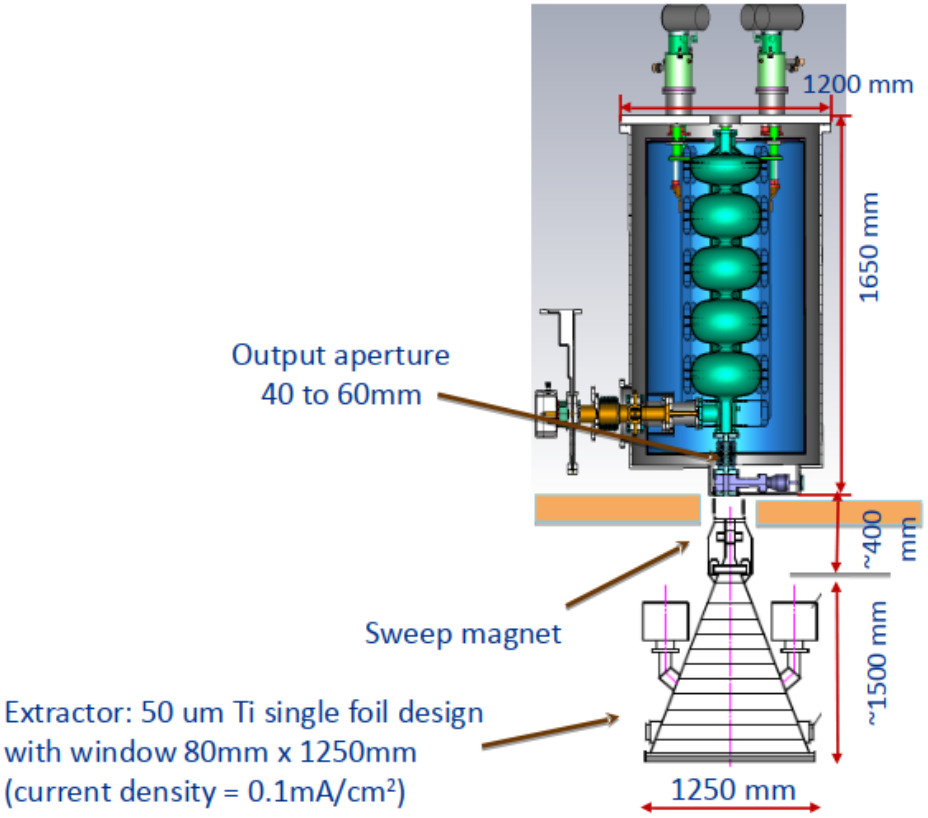

Figure 20 A schematic of the SRF cryomodule and the beam delivery system.

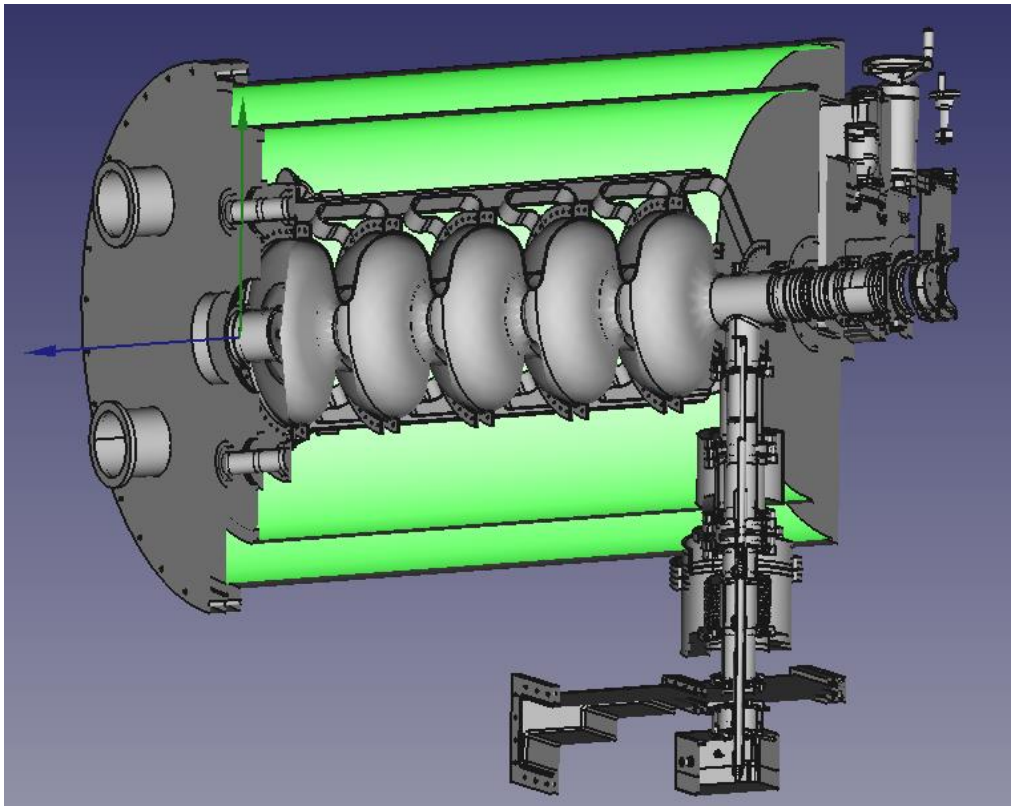

Figure 21 CAD model of the cryomodule

Figure 21 illustrates a cryomodule used to generate a realistic 3D MARS15 model that included all necessary details about the geometry, materials, and electromagnetic fields. Energy deposition for the downstream windows and radiation loads to the SC cavities due to backscattering for different materials and thicknesses were calculated. Electromagnetic showers were modelled in the EGS5 mode down to 1 keV. Photo-neutron production was enhanced using the native biasing and branching techniques of MARS15 [23], with neutrons followed down to 1 millielectronvolt.

CHOICE OF WINDOW MATERIAL

To identify the best choice for the window material, IARC compared the performance of Beryllium (Be), Aluminum (Al), Titanium (Ti) and Stainless Steel. The beam power deposition density and back-scattering of particles were estimated for each respective material. To do this, the team modeled a broad electron beam. Beam power deposition density was evaluated for each material. "Broad beam" in radiation penetration studies entails modeling an infinitely wide beam irradiating an infinitely wide layer of material. Figure 22 shows the beam power deposition density through different materials for 1MeV and 10 MeV beam. Average current density in this study was assumed to be $1mA/cm^2$. It can be observed that power deposition density for Ti is lower at 10 MeV than 1 MeV.; this is because radiation interaction increases with beam energy, creating bremsstrahlung photons that escape through the window without depositing their energy. Though power deposition density decreases at higher energy, bremsstrahlung photons increase the likelihood of neutron production and generate an electromagnetic shower. The physical properties of Ti— combined with

experience derived from existing Ti windows developed for a 1MeV beam at Novosibirsk— favors a Ti window [24]. Ti windows are commercially available and reduce the technical risk.

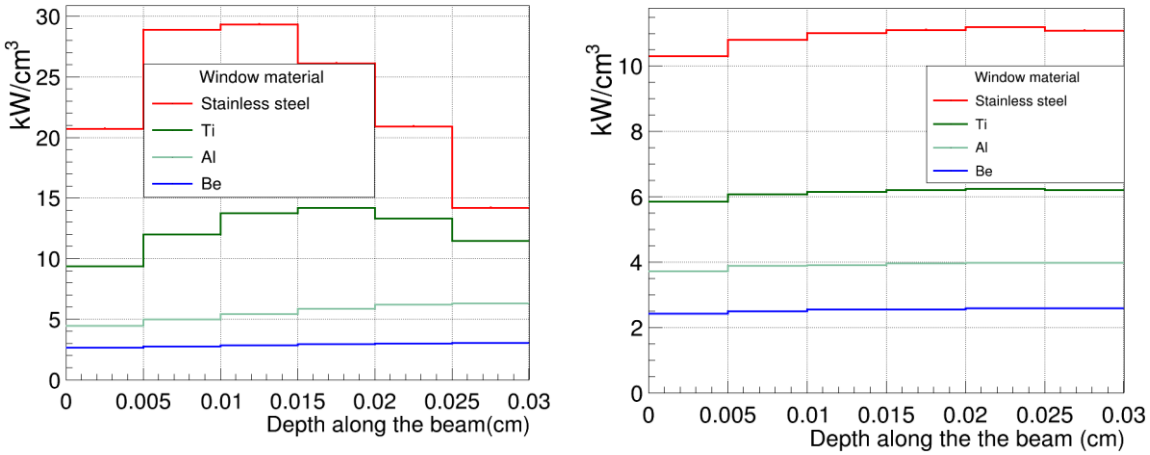

Figure 22 Power deposition density in different window materials irradiated by a broad electron beam with energy of 1 MeV (left) and 10 MeV (right). The average current density is assumed to be 1 mA/cm². Note that initial thickness of the material was not zero in the simulation.

IMPLICATION OF MATERIAL THICKNESS

Back-scattering from the windows might result in an increase in the radiation load to the SRF cavity. Thus, the effect of Ti window thickness was evaluated.

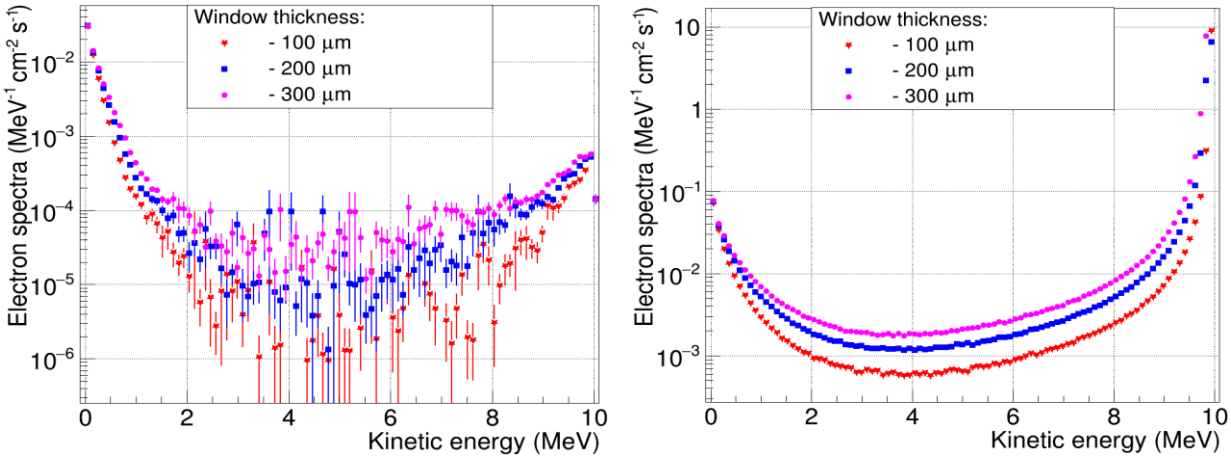

Figure 23 Electron/positron spectra escaping from a downstream Ti-window of different thicknesses in the backward (left) and forward (right) direction for a broad 10-MeV electron beam irradiation.

Figure 23 shows the energy spectra of electrons and positrons emitted in the backward and forward direction after 10 MeV broad beam irradiation of Ti-windows with thicknesses of 0.1, 0.2 and 0.3 mm. Figure 24 shows photon spectra for the same arrangement. Most of the photons have energy below 2 MeV. However, maximum photon energy is as high as the beam energy. In medium-Z and high-Z materials, these photons can generate noticeable fluxes of long-range neutrons, which could result in an elevated radiation level in the irradiation enclosure. This could increase the shielding requirements of the facility.

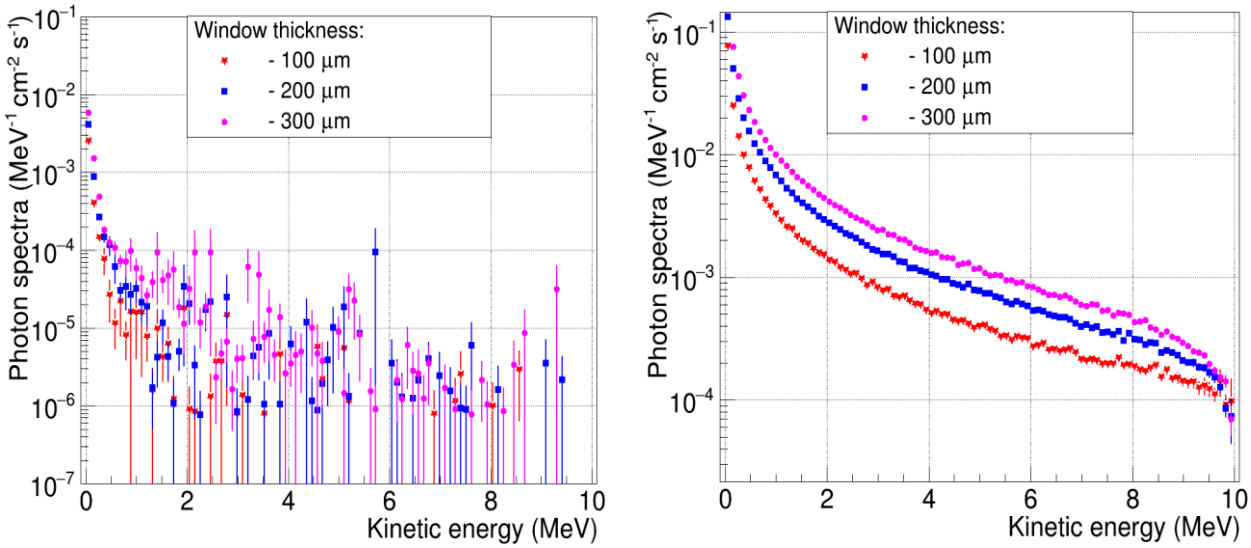

Figure 24 Bremsstrahlung photon spectra escaping from the downstream window of different thickness in the backward (left) and forward (right) direction for a broad 10-MeV electron beam irradiation.

Figure 25 shows the photon energy thresholds for production of neutrons. This demonstrates the neutron production threshold for Ti is below 8 MeV and suggests long range particles will be produced via the interaction of a 10 MeV beam with a Ti window.

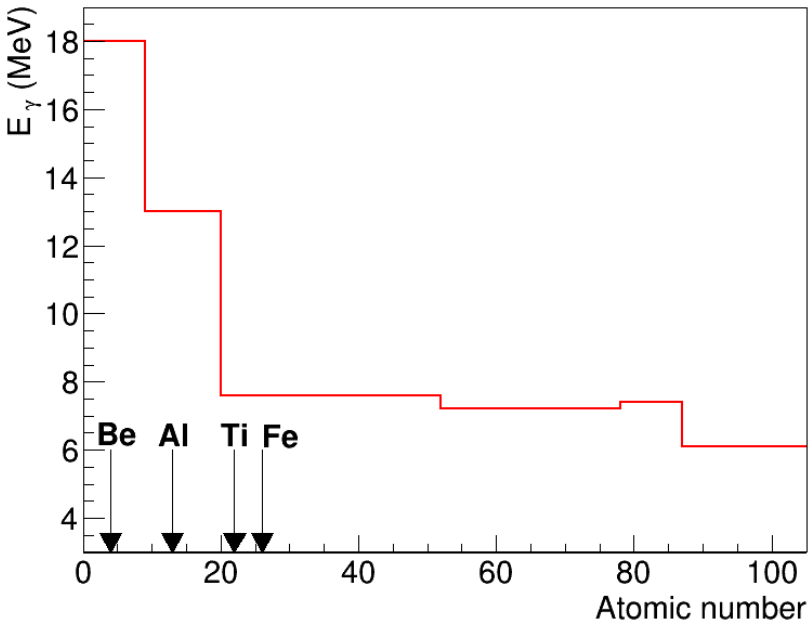

Figure 25 Photon-energy threshold for neutron production in photo-nuclear reactions as a function of atomic number.

COST ANALYSIS

Cost analysis for the machine is segmented into two parts: the construction cost and the operating cost.

CONSTRUCTION COST

The construction cost for the first article includes professional services (labor) required for R&D of critical components such as the superconducting cavity, RF gun design etc. and the purchasing and fabrication expenses of components and their associated systems, such as a beam position monitor and its associated electronics. First, the construction cost of a linac module was estimated. The construction cost of each section is summarized in Figure 26. Commissioning of the linac requires support from a technician, engineers (e.g., electrical engineers, mechanical engineers, etc.), and managers to execute timely commissioning. A commissioning cost was added, which yields a total construction cost of ~$ 7.8 M for a single 1 MW linac module. Figure 27 shows the distribution of the construction cost for the very first 1 MW linac module.

Injector Section	**Quantity**	**($k)**
RF Gun	1	308
Injector Cavity	1	60
Power Coupler	1	65
RF Source	1	250
Total		**$ 976.75 k**

Accelerator Section	**Quantity**	**($k)**
Solenoid	1	92.25
Solenoid Power Supply	1	59.2
Corrector Assembly	1	49
SC Cavity	1	520
Power Coupler	1	272.75
Cryostat	1	523.7
RF Source	1	2300
Cryo-cooler	3	470
Interlocks	-	175

Gate Valves	2	37.6
Vacuum Pump*	3	68.3
BPM System	1	44.5
Total		**$ 4643 k**

* Three vacuum pumps to be placed at end of the injector section, in cryomodule and at DPI.

Beam Delivery	**Quantity**	**($k)**
Vacuum Pump	2	36.8
Sweeping Magnet	1	203.75
Magnet Power Supply	1	67.25
Water Chiller System	1	34.2
Ti Window	1	53.75
Faraday Cup	1	1.15
Radiation Monitoring and Safety	-	107.5
Total		**$ 504.4 k**

Figure 26 A preliminary cost estimate for a single linac module for a 10 MW beam facility. This cost comprises both material and labor expenses.

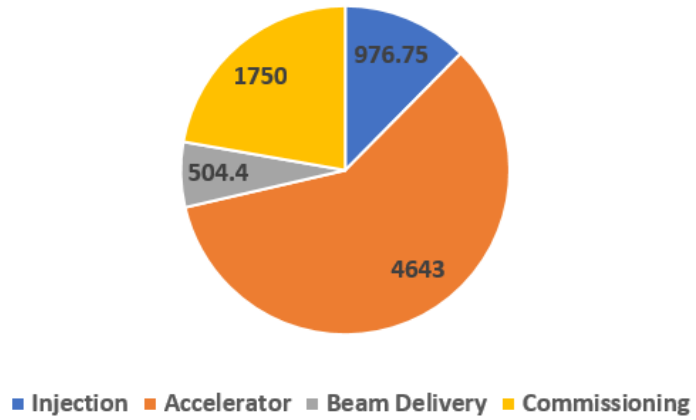

Figure 27 Distribution of a total of $ 7.8 M of construction cost of the very first 1 MW linac module. Each number is presented in unit of $k ($1k=$1000).

Experience with a similar project (LCLS-II cryomodule) suggests that fabrication of a very first module is more expensive than its industrial production version, as the first module includes the labor costs associated with R&D to finalize design specifications. From the cost estimate for the Proton Improvement Plan (PIP II) linac at Fermilab, which also uses 650 MHz, one can estimate

that the rest of the nine linac modules will be 50 % cheaper than the first module. Using this approach and including one-time construction costs accounting for civil work, radiation shielding, and procurement costs, a total cost of the 10 MW facility comes to ~45.4 M. Figure 28 summarizes the total construction cost of a 10 MW facility.

		Quantity	($M)
One-time Construction Cost	Civil Work	-	0.84
	Radiation Shielding	-	1.09
	Procurement Cost	-	0.15
Linac Module	First Linac Module	1	7.87
	Nine Linac Module	9	35.4
	Two spare modules	2	7.87
Total Cost of facility			53.27

Figure 28 Construction cost of a 10MW accelerator facility

OPERATION COST

Operating cost for the facility was projected by determining the operating cost of a single module and scaling it up for the complete facility. The operating cost for the 1 MW accelerator can be segmented into electricity cost, maintenance/repair cost, and labor cost. The electricity cost for the machine arises from operating the cryo-coolers and operating the RF power system. Since a water treatment facility will be operational 24/7, one must add redundancy to the design. The previous report indicated the need for one module for every five modules to act as a backup. Therefore, the 10 MW scheme requires two extra modules as a standby in case of repair or maintenance in another module. For the reliability calculation for the SRF module, refer to the previous report [1]. It was assumed that 1% of the capital cost (typically through service contract) goes toward maintenance and repair. For labor, an average of one full-time operator and one part-time engineer for day-to-day operation of the machine was assumed, which amounts to ~$150K per year of labor.

To estimate electrical power, the team assumed a 1 MW RF power module operating at 75% efficiency. This requires about 1.34 MW of electricity. Continuous operation over one year (8,670 hrs) of an RF power module requires 1.17E7 kWh (units) of electricity. Next, each of the three cryocoolers requires 15 kW electrical input, which sums up to 3.94E5 kWh of electricity over one year of cryocooler operation. Taking the unit price of industrial electricity to be 5.8 cents/kWh (average for Illinois [25]) the yearly cost of operation of one 1 MW accelerator module is $700k. Scaling from 1 MW to 10 MW, the total electricity cost is estimated to be $7M per year of continuous operation. Including $150k for operational labor, the annual operating cost for the 10 MW facility is estimated to be $7.15M. This is equivalent to $816/hr of operating cost. Note that as much as 97% of this electricity goes into the RF power supply and merely 3% is needed for cryocoolers; therefore, adding two spare modules, which are cold (no RF), increases the total operational budget to $818.5 per hour.

A 10 MW facility will be able to treat 1000 kg of material per second with a dose of 10 kGy, if the beam is fully absorbed by the biosolids. This is equal to 3.6E6 kg/hr of throughput. Based on

$818.5hr treating 3.6E6 kg/hr of throughput, the cost of biosolid treatment is 0.023 cents/kg.

Additional R&D and Technology Development Needed for Compact SRF Accelerator:

To transition lab developed breakthroughs in SRF into a viable MW class industrial accelerator, several key technologies require further development. In what follows, it is assumed the goal is an SRF based module capable of producing ~ 1 MW or more CW beam for use in either fixed or mobile applications. The enabling R&D topics are:

MULTI-WATT CRYOCOOLER DEVELOPMENT AND DEMONSTRATION

Conduction cooling of SRF cavities is a Fermilab proprietary technology (US Patent 9,642,239 B2) that, when combined with commercial cryocoolers, enables SRF cavity operation without liquid cryogens. This novel and proprietary configuration (US Patent 10,070,509 B2) results in dramatic reductions in complexity, size, weight, and cost. However, existing cryocoolers cannot go beyond 2.5 W at 4K. There is a significant need for higher capacity cryocoolers to reliably support a heat budget of ~10 W at 4 K. As of this report, it is known that a 3W cryocooler could be available commercially in 2019.

Status: In 2018, Fermilab demonstrated this technology at 650 MHz with a gradient of 1-2 MV/m using a 1W cryocooler. This was developed as a part of the Laboratory Directed Research and Development Program. An increase in gradient will require a larger cryo-cooler capacity.

Need: Further R&D of conduction cooling and multi-W cryocoolers can provide a huge benefit by simplifying the cryo-design, lowering costs, and advancing the design toward commercial viability. R&D is needed to develop cavities optimized for conduction cooling, develop cavity and coupler heat removal systems optimized for conduction, and to fund first purchases from vendors willing to develop 4K cryocoolers with higher capacities (~ 10 W).

MULTI-CELL Nb_3Sn COATED CAVITIES

An optimized, magnetically shielded, high Q_0, 650 MHz Nb_3Sn coated 4 ½ cell cavity can achieve dynamic RF losses ~2.5 W at 4.5K when operated CW. This is a factor of 20 better than can be currently achieved with a pure Niobium (Nb) cavity when operated at 4.5 K. It is Nb_3Sn technology that enables one to envision a simple industrial SRF accelerator cooled with commercial cryocoolers and without liquid Helium. Development of Nb_3Sn coated cavities is a high priority.

Status: Single cell 1.3 GHz Nb cavities coated with Nb_3Sn have been demonstrated and have achieved quality factor (Q) ~ 2×10^{10} at 4K. Most recently, Fermilab demonstrated 650 MHz coated single cell cavities.

Need: Development of a reproducible cavity coating process that can be transferred to industry requires research on the Nb_3Sn coating properties and defects, development of coating infrastructure including high temperature vacuum ovens, and funds for sufficient cavity throughput such that a

robust process can be developed in a timely way. A program to coat multi-cell 650 MHz Nb3Sn cavities is needed. After achieving success in the lab with high Q_0 650 MHz Nb3Sn "multi-cell" prototype cavities, the cavity treatment must be further developed into a robust industrial process and transferred to industrial cavity manufacturers.

RF POWER SOURCE

Broad adoption of this accelerator for wastewater treatment requires an affordable, high-efficiency (> 80%), high-power RF power source. However, continuous Wave (CW) RF power sources with 50% wall plug power efficiencies are commercially available at ~ $ 10/watt. These would be suitable for testing the first article accelerator. Fermilab has developed a patent-pending magnetron-based RF system capable of fast slew rates and precise control of the power and phase while dramatically reducing the cost per watt of continuous-wave RF power systems (US Patent Application 2017/0280549A1).

Magnetrons were developed pre-World War II for radar applications. However, even today they remain the most efficient source for the generation of RF power in the hundreds of MHz to a few GHz frequency range. Industrial RF heating systems employ 100 kW, CW, 915 MHz magnetrons and achieve high reliability at < $1 per watt of output RF power. Driving an SRF-cavity based accelerator will require more complex controls and better spectral purity of the RF output.

Need: The first step is to engage an existing RF tube manufacturer to scale existing 915 MHz or 1.3 GHz magnetron designs to 650 MHz and build the first article high-power (>150kW) CW magnetron. The next step is for a vendor to integrate one or more of these tubes into an efficient high power (~ 300 kW) commercial CW RF power source. Development of this 650 MHz RF source is a long-lead item that is currently not funded from any source

HIGH CURRENT SRF INJECTOR DESIGN

Injecting a high current electron beam with minimal particle loss into an accelerator is challenging. The simulation shows external injection is superior to integrated gun design at high-power levels [> few MW], where dynamic losses could adversely affect accelerator operation.

Need: A high power 650 MHz SRF injector design and experimental facility is the next logical step. Such a facility could be used to optimize the gun design for the proposed accelerator. It can also serve as a long-term test bed for SRF compatible cathode development. A 2nd harmonic RF system on the gun could lead to very high beam transmission and low beam power losses to cold cavity surfaces.

Summary and conclusion

This report presents a conceptual design for a 10 MW accelerator system for a wastewater treatment facility such as the MWRD plant. This facility included ten identical linac modules and two spares; each module, when active, will deliver 1 MW beam power. All active modules will operate simultaneously to deliver a combined 10 MW of beam power. A baseline configuration of a 1 MW linac module was developed to deliver a 100 mA, 10 MeV electron beam in the CW regime. Optimal

choices of nominal operating parameters of the beamline elements were made using beam dynamics simulations. A preliminary electromagnetic design of critical elements such as the RF gun, injector cavity, and SRF cavity were also performed. To achieve a reliable operation of the linac, it is essential to limit total power deposition (static and dynamic losses) to below 1 W and 10 W at 4K and 70 K. This was achieved by reducing beam loss on the cold surface.

As detailed in the cost section, it appears that the conduction cooling scheme using cryocoolers will become costly and complex beyond the 10 W per module heat budget requirement when compared to a 4K plant, which can offer much higher cooling capacity for a 10 MW accelerator that will need several 10's of Watts. Therefore, for a 10 MW facility— even if the losses are significantly controlled to less than 10^{-6}— the losses are dominated by RF compared to beam loss at these power levels and it is simpler to take advantage of the economies of scale of a liquid Helium plant. However, the work also indicates that if external injection is used, a single 1 MW SRF module based on conduction cooling is preferable to separate 250 kW modules, thus dramatically decreasing the footprint of the overall system.

A detailed study was performed using MARS15 to optimize the window material. It was observed that beam power deposition density for a Titanium window was smaller for 10 MeV beam irradiation compared to 1 MeV beam for the same current density. Titanium windows have already been demonstrated for use with 1 MeV beam; thus, Titanium was selected for the window material.

The construction and operational costs of the facility were projected. Cumulative experience with building such projects suggested that the construction of a first article 1 MW linac module would be expensive compared to its industrial production version. Based on prior experience from the PIP-II linac, the building cost of a 10 MW accelerator facility was estimated to be $ 53.27 M including spare modules for high availability. Note that a liquid He cryosystem would be better than a conduction cooled configuration when the losses are more than 10 W per module. Further developments in high-Q SRF cavity R&D at modest gradients can substantially modify the cost of a facility.

REFERENCES

1. Link to the CRADA protected document is available from the DOE Accelerator Stewardship Program Manager. Title of the proposal is: "CONCEPTUAL DESIGN OF AN ELECTRON ACCELERATOR FOR BIO-SOLID WASTE TREATMENT".
2. IAEA, Working Material – Prospects and Challenges in Application of Radiation for Treating Exhaust Gasses, pg 9, Vienna, Austria, (2011)
3. IAEA, "Emerging Applications of Radiation Processing," IAEA-TECDOC-1386, Vienna, Austria, (2004)
4. IAEA, "Radiation Treatment of Gaseous and Liquid Effluents for Containment Removal," Proceedings of a technical meeting, Sofia, Bulgaria, (2004)
5. DOE Report "Workshop on Energy and Environmental Applications of Accelerators" (2015)
6. R. Kephart et. al., Proceedings of IPAC2017, Copenhagen (2017)
7. A. Arnold and J. Teichert, Overview on superconducting photoinjectors, Phys. Rev. ST Accel. Beams 14, 24801 (2011).
8. J. Madey, G. Ramian, and T. Smith, A fast pulsed electron gun system, IEEE Trans. Nucl. Sci. 27, 999 (1980).
9. D. Oepts, A. van der Meer, and P. van Amersfoort, The free-electron-laser user facility FELIX, Infrared Phys. Technol. 36, 297 (1995).
10. V. Bolotin et al., Status of the Novosibirsk terahertz FEL, Nucl. Instrum. Methods Phys. Res., Sect. A 543, 81(2005).
11. http://www.cathode.com/
12. https://www.comsol.com/
13. V.N. Volkov et. al, "CW 100 kev Electron RF Injector For 40 mA Average Beam Current"
14. Code SUPERSAM for calculation of electron guns with high beam area convergence - Myakishev, D.G. *et al.* Int.J.Mod.Phys.Proc.Suppl. A2B (1993) 915-917
15. http://irfu.cea.fr/en/Phocea/Page/index.php?id=780
16. P.N. Ostroumov, K.W. Shepard, S.H. Kim, E.S. Lessner, R. Laxdal, R. Wheatley, "A New Generation of Superconducting Solenoids for Heavy-Ion Linac Application", LINAC2003,Gyeongiu.
17. G. Davis, et al, "Designing Focusing Solenoids for Superconducting RF accelerators", IEEE Transactions on Applied Superconductivity, vol. 17, no. 2, pp. 1221 – 1224, June 2007.
18. "Resonant interaction of the electron beam with a synchronous wave in controlled magnetrons for high-current superconducting accelerators" Phys. Rev. Accel. Beams 21, 062001, 14 June 2018
19. https://www.cpii.com/docs/datasheets/264/ECONCO%20%20100L%20Magnetron-new%20photo.pdf
20. http://www.capp.iit.edu/workshops/epem/Transparencies/Guidee.pdf

21. M. Boyle *et al.*, "L3 L6200 Multibeam IOT for the European Spallation Source," in *IEEE Transactions on Electron Devices*, vol. 65, no. 6, pp. 2096-2100, June 2018.

22. A. Saini, V. Labedev, N. Solyak and V. Yakovlev, "Estimation of Cryogenic Heat Loads in Cryomodule due to Thermal Radiation," in form of proceedings of IPAC2015, held in Richmond, USA from May 3 08 2015.

23. N.V. Mokhov, "MARS Code System User's Guide", Fermilab-FN-628 (1995)

24. J.I. Golubenko, N.K. Kuksanov, P.I. Nemytov, "Powerful electron accelerator ELV-12 for ecological applications: power supply and control". Budker Institute of Nuclear Physics.

25. https://www.electricitylocal.com/states/illinois/chicago/

Appendix

A study was performed to benchmark SMASON with a 3-D code MICHELLE. Figure 1 shows a gun geometry and particle emission from cathode for respective codes.

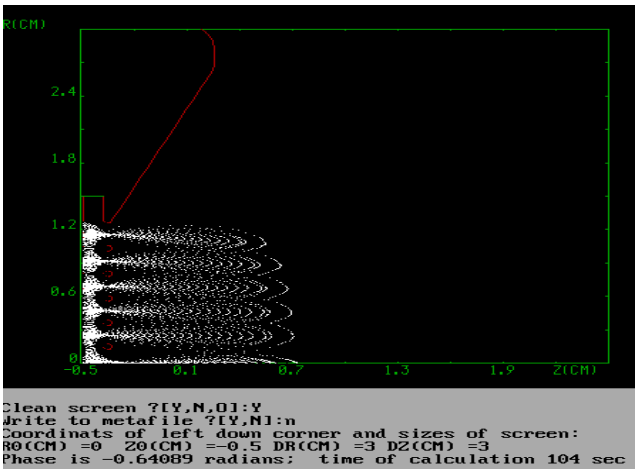

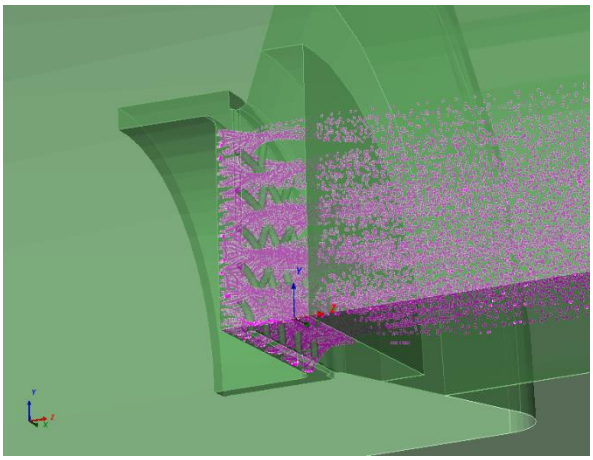

Figure 1: 2D (left) and 3D (right) geometries of the gun used in SMASON and MICHELLE respectively.

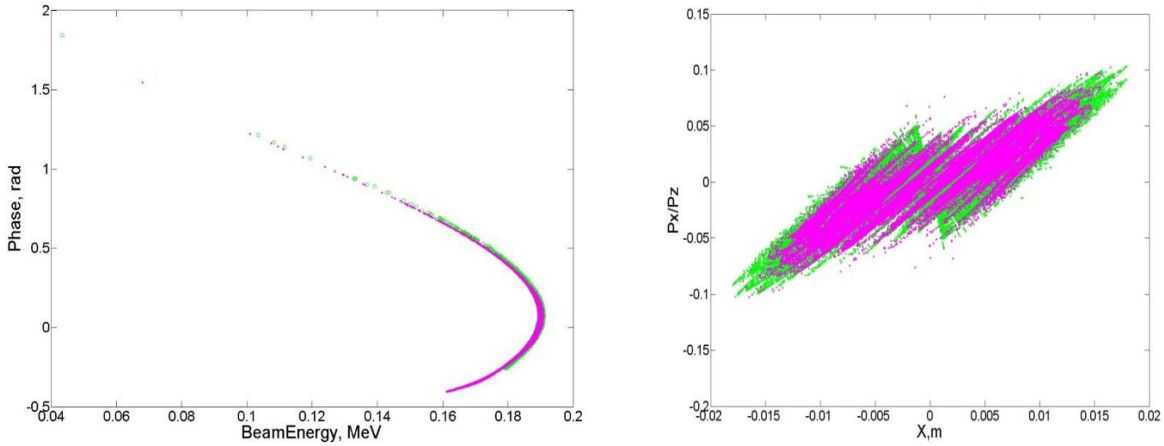

Figure 2: Longitudinal (left) and transverse (right) phase space distribution at the exit of the gun obtained from MICHELLE (magenta) and SMASON (green). Input parameters were same for both codes

A comparison of phase space distribution at the end of the gun obtained from MICHELLE and SMASON was shown in figure 2. One can observe that both codes agreed well.